Available online at www.sciencedirect.com
ScienceDirect
Nuclear Physics B Proceedings Supplement 00 (2014) 1–7
Nuclear Physics B Proceedings Supplement

Measurement of Jet Production Properties in pp Collisions with the ATLAS Detector

B. Malaescu On behalf of the ATLAS Collaboration

Laboratoire de Physique Nucléaire et des Hautes Energies, IN2P3-CNRS et Universités Pierre-et-Marie-Curie et Denis-Diderot, 75252 Paris Cedex 05, France

Abstract

Several aspects of the jet production in pp collisions have been measured by the ATLAS collaboration using data collected at the LHC. The measurements of the production cross sections of inclusive, di- and three-jet events probe the dynamics of QCD and can constrain the parton proton structure. The cross sections are measured using jets clustered with the anti-k_t algorithm with different distance parameters and compared to expectations based on next-to-leading order QCD calculations, corrected for non-perturbative and electroweak effects, as well as to next-to-leading order Monte Carlo simulations. Ratios of inclusive cross sections measured at different centre-of-mass energies allow for reduced experimental and/or theoretical uncertainties. Double-differential dijet and three-jet cross sections have been measured in proton-proton collisions at 7 TeV as a function of di- and three-jet masses and the jet rapidity separation. An NLO QCD analysis of the data indicates constraining power for parton distribution functions of the proton.

Keywords: QCD, jets

1. Introduction

The inclusive jet, dijet and three-jet cross sections are important tools for testing Quantum Chromodynamics (QCD) and searching for physics beyond the Standard Model at the LHC. Data collected using the ATLAS detector [1] have been used for performing this type of measurements.

The ATLAS Collaboration has published a first set of measurements of the inclusive jet and dijet cross sections at $\sqrt{s}$ = 7 TeV, using an integrated luminosity of 17 nb^{-1} [2]. A second set of measurements [3], using the full 2010 data sample, significantly extended the covered phase-space, due to the enhanced integrated luminosity of 37.3 pb^{-1}. The inclusive jet cross section has also been measured with a data sample of 0.2 pb^{-1} at $\sqrt{s}$ = 2.76 TeV, and a comparison with the inclusive jet measurement at $\sqrt{s}$ = 7 TeV has been performed [4]. The measurement of the dijet [5] and of the inclusive jet [6] cross sections using 4.7 fb^{-1} in the full 2011 data sample at $\sqrt{s}$ = 7 TeV show an improved precision comparing to the previous measurements. A preliminary measurement of the three-jet cross section [7], performed using the same data sample, has also been presented for the first time at this conference. These analyses probe next-to-leading order (NLO) perturbative QCD and parton distribution functions (PDFs), being also sensitive to potential New Physics (NP) contributions, in a kinematic regime not explored before.

2. Jet definition, reconstruction and calibration

For the ATLAS inclusive jet and dijet cross section measurements, jets are defined using the anti-k_t algorithm [8]. The measurements are performed for two different values of the distance parameter R (0.4 and 0.6).

Jets are reconstructed from three-dimensional topological clusters built from calorimeter cells. The topological clusters are calibrated at the electromagnetic scale, which correctly reconstructs the energy of the electromagnetic showers deposited in the calorimeter.

For the measurements based on the 2011 data at $\sqrt{s}$ = 7 TeV, a correction is applied to the energy of the topological clusters identified as hadronic by their topology and energy density. It accounts for calorimeter response, dead material and out-of-cluster losses for pions, allowing to improve the energy resolution and to reduce the response dependence on the jet flavor.

The four-momentum of the uncalibrated jet is defined as the sum of the four-momenta of its constituent calorimeter energy clusters. Additional energy due to pile-up interactions is subtracted by applying a correction depending on the number of reconstructed vertices in the event and the average number of collisions per bunch crossing. This correction is derived in Monte Carlo simulation (MC) and validated in data, while the stability of the measurements under the pile-up conditions is also checked. The direction of the jet is corrected such that it originates from the selected hard-scatter vertex in the event. The MC simulation is then used to correct the energy of the jet for instrumental effects like energy lost in the dead material or due to calorimeter non-compensation. An additional *in-situ* calibration, derived combining results of $\gamma-$jet, Z-jet and multijet momentum balance techniques, is applied for the 2011 measurements at $\sqrt{s}$ = 7 TeV, to correct for residual differences between MC and data. The full calibration methods used for the 2010 and 2011 datasets are described in detail in ref. [9, 10].

The jet energy scale (JES) uncertainty is the dominant uncertainty for the inclusive jet, dijet and three-jet measurements [5, 6, 7, 10]. Comparing to the previous measurement [2, 3], this uncertainty has been strongly reduced, due to the use of *in-situ* calibration methods. The JES uncertainty has been split in several components (sources), treated as fully correlated in p_T and rapidity, and independent between each other. This allows for a reliable treatment of the bin-to-bin correlations of the uncertainties for a given measurement, and to keep track of the correlations between measurements. Because the potential correlations between the various uncertainty components are not perfectly known, two additional JES uncertainty configurations are considered, with *stronger* and *weaker* correlations comparing to the nominal one.

3. Data correction to particle level

The measured cross sections are corrected for the experimental effects and are hence obtained for the *particle level* final state. In MC particle jets are built from stable particles, including muons and neutrinos from decaying hadrons.

The inclusive jet, dijet and three-jet measurements are corrected from detector to particle level using the matrix-based IDS [11] unfolding method. A transfer matrix relating particle level and reconstructed quantities is built from MC, using a geometrical matching between particle level and reconstructed level jets. The matching efficiency is taken into account in a three step unfolding procedure. The first step applies the matching efficiency at the reconstructed level to the data spectrum, so that it can be directly compared with the spectrum of MC matched reconstructed jets. The second step performs the actual unfolding, correcting for the transfer of jets (events) between the bins. A local, significance-based regularization is used in IDS at this step. Finally, the third step corrects for the matching efficiency at the particle level.

The potential bias of the unfolding method has been studied using a data-driven closure test, relying on the shape comparison between data and MC at the reconstructed level. For this test, a reweighting of the particle level MC spectrum (used to build the transfer matrix) by a smooth function is performed, such that, after projection on the reconstructed MC axis, a better agreement with data is observed. The reweighted reconstructed MC is unfolded, using the original transfer matrix (without reweighting, like for the unfolding of the data) as input of the IDS method. The comparison of the corresponding results with the reweighted particle level MC provides an estimation of the *MC shape uncertainty*. The uncertainty obtained using the IDS method is at the 1% level, much smaller than the other systematic uncertainties affecting the measurement.

The full set of uncertainties are propagated from the reconstructed to the unfolded level. The statistical uncertainties are propagated using pseudo-experiments, where both the input data spectrum and the MC transfer matrix are statistically fluctuated, the unfolding is redone and a covariance matrix is obtained. Each event is fluctuated following a bootstrap method, using a Poisson distribution with a mean of one before applying any additional event weights. The pseudo-random Poisson distribution is seeded uniquely for each event, so that the full information on the statistical correlations between the various measurements is propagated. Each component of the systematic uncertainty is propagated by performing shifts of the reconstructed spectrum by one standard deviation in the positive and negative direction respectively, redoing the unfolding and comparing the results with the nominal unfolded spectrum. In addition, for the 2011 inclusive jet cross section measurement [6], shifts of 1, 2 ... 5 standard deviations have been performed and propagated. This study has shown that a

log-normal shape provides a better description of the distribution of the systematic uncertainties of the cross section, compared to a Gaussian. The resolution uncertainty is propagated by performing a smearing of the nominal transfer matrix by the resolution uncertainty, re-doing the unfolding and comparing with the nominal result. The bootstrap method has also been used for evaluating the statistical significance of the propagated systematic uncertainties.

4. Frequentist method for data/theory comparison

The advantage of the comparison between data and theoretical predictions at the particle level rather than at the reconstruction level is that data can be used to test any theoretical model without the need for further detector simulation. As the additional uncertainties introduced by the unfolding procedure are small, they do not have a significant effect on the power of the comparison. The frequentist method described in Ref. [5] provides quantitative statements about the level of agreement between the Standard Model (SM) predictions and the measured cross-sections. The test statistic exploited there is a generalized χ^2, simultaneously accounting for the correlations of the statistical and systematic uncertainties (both theoretical and experimental), as well as their asymmetric distributions.

A large set of pseudo-experiments that represent fluctuations of the theory hypothesis due to the full set of experimental and theoretical uncertainties allow to obtain the χ^2 distribution expected for experiments drawn from the parent distribution of a given theory hypothesis. Depending on the study being carried out, the theory hypothesis can be the SM, or the SM with any of its extensions. For each pseudo-experiment, the χ^2 value is computed between the pseudo-data and the theory hypothesis. In this way, the χ^2 distribution that would be expected for experiments drawn from the theory hypothesis is obtained without making assumptions about its shape. The *observed* χ^2 ($\chi^2_{\rm obs}$) value is computed using the data and the theory hypothesis. To quantify the compatibility of the data with the theory, the ratio of the area of the χ^2 distribution with $\chi^2 > \chi^2_{\rm obs}$ to the total area is used. This fractional area is called a p-value. If the observed p-value is smaller than 5%, the theoretical prediction is considered to poorly describe the data at the 95% CL.

An extension of this frequentist procedure [5], based on the CLs technique [12], is used to explore potential deviations in dijet production due to contributions beyond the SM. This method accounts for cases where the measurement has little sensitivity to the the signal, which is small compared to the background.

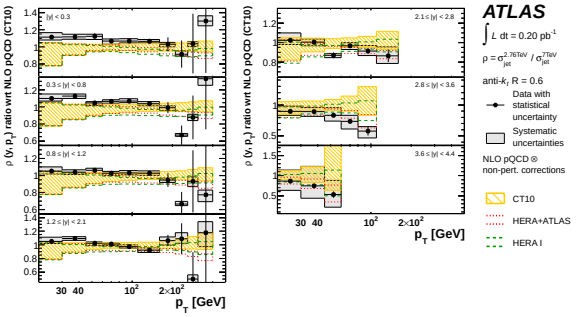

Figure 1: Comparison of NLO pQCD predictions of the jet cross-section ratio of $\sqrt{s}$ = 2.76 TeV to $\sqrt{s}$ = 7 TeV calculated with the CT10 PDF set, the fitted PDF set using the HERA data only and the one using HERA data and the ATLAS jet data with R=0.6 [4]. The predictions are normalised to the one using the CT10 PDF set. Also shown is the measured jet cross-section ratio. The 4.3% uncertainty from the luminosity measurements is not shown.

5. Theoretical predictions and comparison with the data

The unfolded experimental cross sections are compared with the NLO QCD prediction, corrected for non-perturbative effects. Both the NLOJET++ [13] and the POWHEG [14, 15] (with parton shower switched off) generators were used for the hard scattering. The uncertainties related to the renormalization and factorization scales, PDFs and α_S are evaluated using APPLGRID [16]. For the theoretical prediction using NLOJET++, the non-perturbative correction factors are derived using PYTHIA [17], while the uncertainties are obtained from comparisons between different PYTHIA tunes, as well as from the comparison with HERWIG++ [18]. The strong dependence of the non-perturbative corrections on the jet-size parameter R, was one of the strong motivations for performing these jet measurements and the comparison with the theory predictions for both $R = 0.4$ and $R = 0.6$. For the most recent measurements [5], corrections for the electroweak tree-level effects of $O(\alpha\alpha_S, \alpha^2)$ as well as weak loop effects of $O(\alpha\alpha_S^2)$ are also applied [19].

The double-differential inclusive jet cross section, as a function of the jet transverse momentum (p_T) and rapidity ($|y|$), has been measured at $\sqrt{s}$ = 2.76 TeV. A comparison with the inclusive jet measurement at $\sqrt{s}$ = 7 TeV has been performed [4]. The systematic uncertainties are strongly reduced for the ratio of the two cross sections, hence the sensitivity to the PDFs (see Figure 1).

Figure 2 shows the double-differential inclusive jet, dijet and three-jet cross-sections for anti-k_t jets with radius parameter R = 0.4, measured at $\sqrt{s}$ = 7 TeV, as a function of the jet transverse momentum and rapidity [6], dijet mass in different ranges of the rapidity separation between the two leading jets (y^* = $|y_1 - y_2|/2$) [5], and three-jet mass in different ranges of Y^* = $|y_1 - y_2| + |y_1 - y_3| + |y_2 - y_3|$ [7] respectively. These measurements cover many orders of magnitude of the cross section values and of the jet transverse momentum, dijet mass and three-jet mass.

A more detailed comparison can be seen in Figure 3, showing the ratio of the NLO QCD predictions with non-perturbative and electroweak corrections to the measurements of the dijet double-differential cross-section. The comparison is performed for various PDF sets: CT10 [20], HERAPDF1.5 [21], epATLJet13 [4], MSTW 2008 [22], NNPDF2.1 [23, 24], NNPDF2.3 [25] and ABM11 [26]. A tension, corresponding to a p-value smaller than 10^{-3}, is observed for the ABM11 PDF set in several phase-space regions. Some tension (p-value smaller than 5%) is also observed for HERAPDF1.5 in some phase-space regions. A good agreement between data and the theory predictions is observed for the other PDF sets. Similar conclusions are achieved for the measurements performed for jets with a size parameter R = 0.6, as well as for the inclusive jet and three-jet (see Figure 4) cross section measurements at $\sqrt{s}$ = 7 TeV.

For the dijet cross section measurement, comparisons have also been performed with the POWHEG prediction, showered with two different PYTHIA tunes [5]. Important differences between these two are observed for jets with R = 0.4, while the differences are smaller for R = 0.6 (see Figure 5).

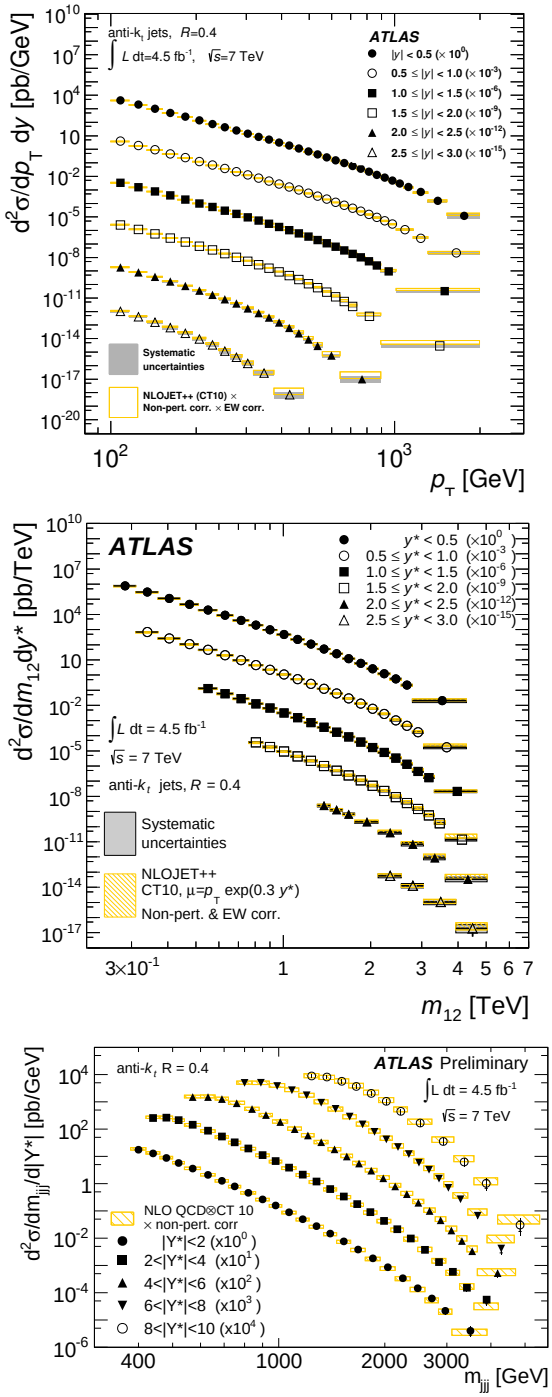

Figure 2: Inclusive jet (top), Dijet (middle) and three-jet (bottom) double-differential cross-sections for anti-k_t jets with radius parameter R = 0.4, shown as a function of the jet transverse momentum and rapidity [6], dijet mass in different ranges of y^* [5], and three-jet mass in different ranges of Y^* [7] respectively. To aid visibility, the cross-sections are multiplied by the factors indicated in the legend. For comparison, the NLO QCD predictions of NLOJet++ using the CT10 PDF set, corrected for non-perturbative (and electroweak in the case of inclusive jets and dijets) effects, are included. The experimental uncertainties (statistical and systematic) and the uncertainty associated with the theory predictions are shown.

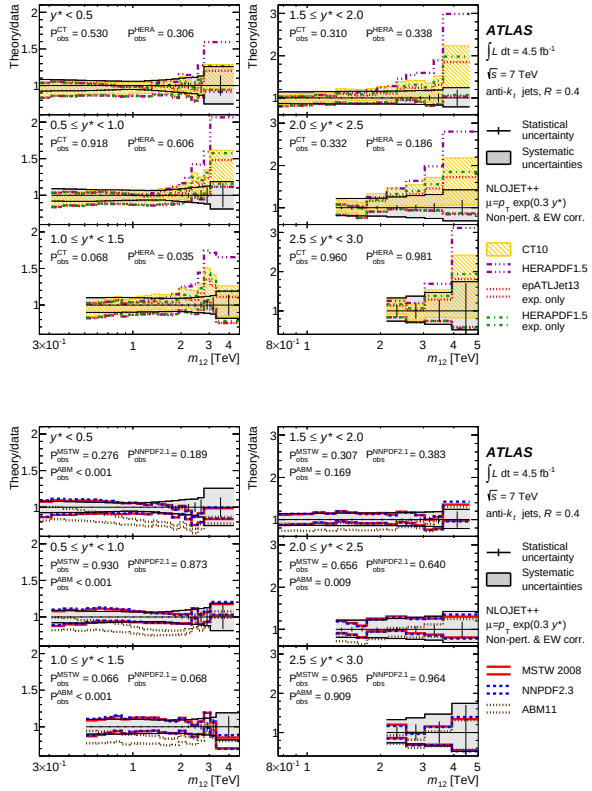

Figure 3: Ratio of the NLO QCD predictions of NLOJet++ to the measurements of the dijet double-differential cross-section as a function of dijet mass in different ranges of y^* [5]. The results are shown for jets identified using the anti-k_t algorithm with radius parameter $R = 0.4$. The predictions of NLOJet++ using different PDF sets (CT10, HERAPDF1.5, and epATLJet13 (top); and MSTW 2008, NNPDF2.3 and ABM11 (bottom)) are shown. Observed p-values resulting from the comparison of theory with data are shown considering all mass bins in each range of y^* separately.

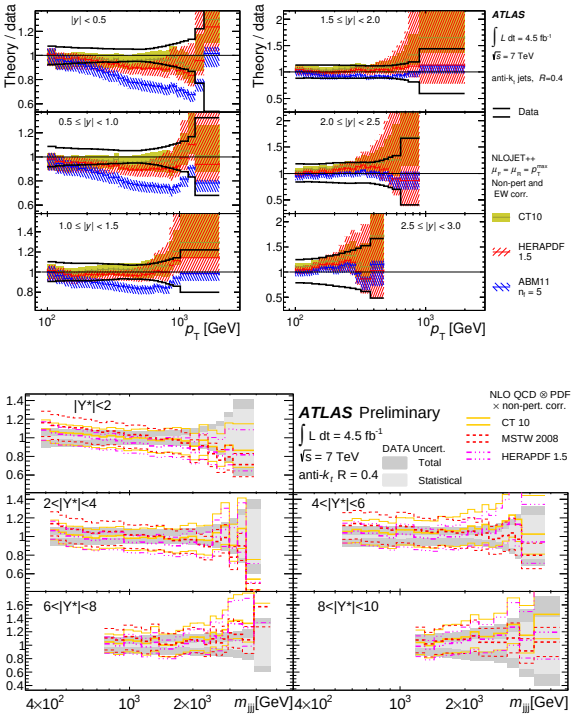

Figure 4: The ratio of NLO QCD predictions, obtained by using NLO-Jet++ with different PDF sets (CT 10, MSTW 2008, HERAPDF 1.5, ABM11) and corrected for non-perturbative (and electroweak in the case of inclusive jets) effects, to the measurements of the inclusive jet (top) and three-jet (bottom) double-differential cross-sections as a function of the jet transverse momentum and rapidity [6], and of the three-jet mass and Y^* [7] respectively. The ratios are shown for jets identified using the anti-k_t algorithm with $R = 0.4$. Data points are always at 1. The experimental uncertainties (statistical and systematic) and the uncertainty associated with the theory predictions are shown.

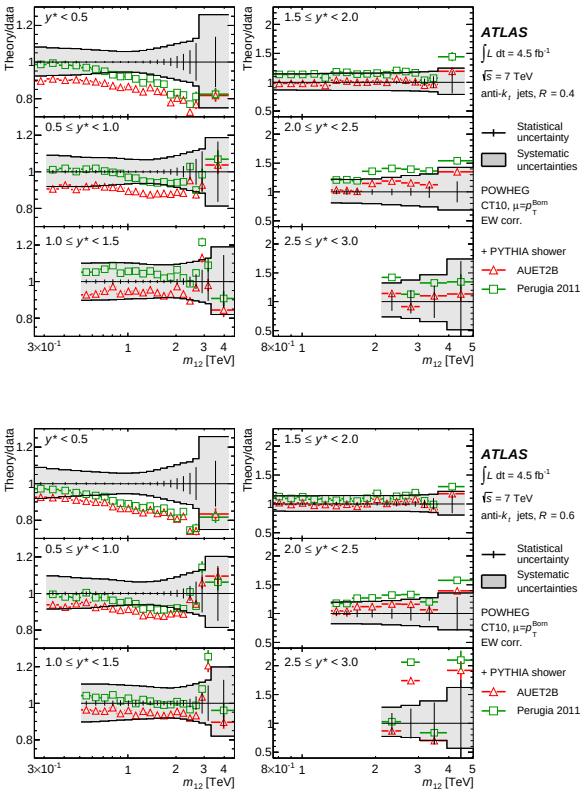

Figure 5: Ratio of the POWHEG predictions to the measurements of the dijet double-differential cross-sections as a function of dijet mass in different ranges of y^* [5]. The results are shown for jets identified using the anti-k_t algorithm with jet radius parameter $R = 0.4$ (top) and $R = 0.6$ (bottom). The predictions of POWHEG with parton-shower MC simulation by PYTHIA are shown for the AUET2B and Perugia 2011 tunes. The statistical (total systematic) uncertainties of the measurements are indicated as error bars (shaded bands).

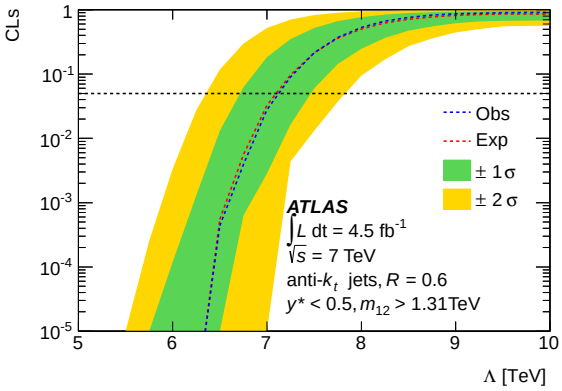

Figure 6: Scan of the CLs value for NLO QCD plus CIs as a function of Λ, using the CT10 PDF set [5]. The green (yellow) bands indicate the $\pm 1\sigma$ ($\pm 2\sigma$) regions. The dashed horizontal line indicates the 95% CL exclusion, computed using the observed (expected) p-value shown by the blue (red) dashed line. The plots correspond to the measurement with jet radius parameter $R = 0.6$ in the range $y^* < 0.5$, restricted to the high dijet-mass subsample.

6. Limits on New Physics using unfolded distributions

To illustrate the sensitivity of the dijet cross section measurement to physics beyond the SM, the model of QCD plus contact interactions (CIs) [27] is considered. In this model, the NP contribution modifies the SM prediction mainly at high dijet mass in the small y^* region, its effect being relatively smaller in other phase-space regions. The PDF sets for which the SM predictions in the region relevant for CI provide a good description of the data are considered: CT10, HERAPDF1.5, MSTW 2008, and NNPDF2.1. The ABM11 PDF set is not considered in this example, because it does not allow to achieve a good description of the data even in the low dijet mass regions where CIs were previously excluded [5].

In order to exclude a range for the compositeness scale, a scan of the observed CLs value (see Section 4) as a function of Λ is performed (see Figure 6). This corresponds to theoretical predictions with jet size parameter $R = 0.6$, using the CT10 PDF set, and exclude the range $\Lambda < 7.1$ TeV at the 95% CL. Similar results are obtained for the other PDF sets considered here, as well as for jets with the size parameter $R = 0.4$. While the expected limits are in the range $7.1 - 7.5$ TeV, the observed ones span the range $6.9 - 7.7$ TeV. It has been checked that the uncertainties on the correlations of the JES uncertainty (see Section 2) has little impact on these results [5].

The results obtained here are similar to the ones obtained by dedicated searches, where a comparison at the reconstructed level is performed between data and the theory predictions folded with detector effects. However, since the information on the unfolded cross sections, their uncertainties and the correlations is publicly available, it is straightforward to apply the method presented here to other NP models.

7. Conclusions

Measurements of the inclusive jet, dijet and three-jet double-differential cross sections have been performed using the full ATLAS datasets at 2.76 and 7 TeV. These measurements are corrected for the detector effects though a matrix-based unfolding procedure. A full propagation of the statistical and systematic uncertainties, together with their bin-to-bin correlations, is performed. This allows to exploit these measurements for constraining PDFs and potential contributions from New Physics.

References

[1] ATLAS Collaboration, 2008 JINST 3 S08003.
[2] ATLAS Collaboration, Eur. Phys. J. C **71**, 1512 (2011) [arXiv:1009.5908 [hep-ex]].
[3] ATLAS Collaboration, Phys. Rev. D **86**, 014022 (2012) [arXiv:1112.6297 [hep-ex]].
[4] ATLAS Collaboration, Eur. Phys. J. C **73**, 2509 (2013) [arXiv:1304.4739 [hep-ex]].
[5] ATLAS Collaboration, JHEP **1405**, 059 (2014) [arXiv:1312.3524 [hep-ex]].
[6] ATLAS Collaboration, arXiv:1410.8857 [hep-ex].
[7] ATLAS Collaboration, ATLAS-CONF-2014-045, https://cds.cern.ch/record/1741019.
[8] M. Cacciari, G. P. Salam and G. Soyez, JHEP **0804**, 063 (2008) [arXiv:0802.1189 [hep-ph]].
[9] ATLAS Collaboration, Eur. Phys. J. C **73**, 2304 (2013) [arXiv:1112.6426 [hep-ex]].
[10] ATLAS Collaboration, arXiv:1406.0076 [hep-ex].
[11] B. Malaescu, arXiv:0907.3791 [physics.data-an]; Proceedings to PHYSTAT2011 workshop, CERN-2011/006, arXiv:1106.3107 [physics.data-an].
[12] A. Read, J. Phys. G: Nucl. Part. Phys. **28** (2002) 2693, http://dx.doi.org/10.1088/0954-3899/28/10/313 .
[13] Z. Nagy, Phys. Rev. D **68**, 094002 (2003) [hep-ph/0307268].
[14] S. Alioli, P. Nason, C. Oleari and E. Re, JHEP **1101**, 095 (2011) [arXiv:1009.5594 [hep-ph]].
[15] P. Nason, arXiv:0709.2085 [hep-ph].
[16] T. Carli, D. Clements, A. Cooper-Sarkar, C. Gwenlan, G. P. Salam, F. Siegert, P. Starovoitov and M. Sutton, Eur. Phys. J. C **66**, 503 (2010) [arXiv:0911.2985 [hep-ph]].
[17] T. Sjostrand, S. Mrenna and P. Z. Skands, JHEP **0605**, 026 (2006) [hep-ph/0603175].
[18] M. Bahr, S. Gieseke, M. A. Gigg, D. Grellscheid, K. Hamilton, O. Latunde-Dada, S. Platzer and P. Richardson *et al.*, Eur. Phys. J. C **58**, 639 (2008) [arXiv:0803.0883 [hep-ph]].
[19] S. Dittmaier, A. Huss and C. Speckner, JHEP **1211**, 095 (2012) [arXiv:1210.0438 [hep-ph]].
[20] H. L. Lai, M. Guzzi, J. Huston, Z. Li, P. M. Nadolsky, J. Pumplin and C.-P. Yuan, Phys. Rev. D **82**, 074024 (2010) [arXiv:1007.2241 [hep-ph]].
[21] H1 and ZEUS Collaborations, HERAPDF 1.5 , H1prelim-10-142, ZEUS-prel-10-018, http://www.desy.de/h1zeus/combined_results/index.php?do=proton_structure.
[22] A. D. Martin, W. J. Stirling, R. S. Thorne and G. Watt, Eur. Phys. J. C **63**, 189 (2009) [arXiv:0901.0002 [hep-ph]].
[23] R. D. Ball, L. Del Debbio, S. Forte, A. Guffanti, J. I. Latorre, J. Rojo and M. Ubiali, Nucl. Phys. B **838**, 136 (2010) [arXiv:1002.4407 [hep-ph]].
[24] S. Forte, E. Laenen, P. Nason and J. Rojo, Nucl. Phys. B **834**, 116 (2010) [arXiv:1001.2312 [hep-ph]].
[25] R. D. Ball, V. Bertone, S. Carrazza, C. S. Deans, L. Del Debbio, S. Forte, A. Guffanti and N. P. Hartland *et al.*, Nucl. Phys. B **867**, 244 (2013) [arXiv:1207.1303 [hep-ph]].
[26] S. Alekhin, J. Bluemlein and S.-O. Moch, PoS LL **2012**, 016 (2012) [arXiv:1302.1516 [hep-ph]].
[27] J. Gao, C. S. Li, J. Wang, H. X. Zhu and C.-P. Yuan, Phys. Rev. Lett. **106**, 142001 (2011) [arXiv:1101.4611 [hep-ph]].